Int J Adv Manuf Technol (2012) 63:109–116
DOI 10.1007/s00170-011-3889-y

ORIGINAL ARTICLE

A novel mathematical model for grinding ball-end milling cutter with equal rake and clearance angle

Fengjun Chen · Sijie Hu · Shaohui Yin

Received: 12 May 2008 / Accepted: 28 December 2011 / Published online: 13 January 2012

Abstract In this paper, new mathematical models and grinding methods of ball-end milling cutter were proposed based on the orthogonal spiral cutting edge curve. In order to avoid interference, a conical wheel was also designed and employed to grind the rake and rear faces of ball-end milling cutter on a five-axis grinder. Mathematical models of both rake face with equal rake angle and rear face with equal clearance angle were established to improve the machining characteristics of ball-end milling cutter. The design and simulation software of ball-end milling cutter was developed to design and optimize different shapes of both rake face and rear face. Furthermore, grinding experiment of the new ball-end milling cutter was carried out to confirm the validation of the mathematical models.

Keywords Ball-end milling cutter · Mathematical model · Rake angle · Rake face · Clearance angle · Cutting edge

1 Introduction

In recent years, as an advanced rotary cutter in current free-form surface machining, the ball-end milling cutter has been widely used in mold/die, aerospace, machinery, and electronics manufacturing fields. High-performance ball-end milling cutters have become more and more important, and the optimize design of the rake face and rear face is also very important for improving machining performance of ball-end milling cutter. The shape of earlier cutting edge was designed into straight line and then improved to be curve and helix. Wu et al. [1–3] designed a cutting edge of "S" shape by defining the included angle between the curve and the cutter axis. Because the helix angle was a constant value, Chen [4] proposed a mathematical solution to the design and manufacturing problems of a cutting edge with constant angle to the axis. He et al. [5] discussed the design and calculation methods on the edge curve of the revolving cutter with equal helix angle. However, the edge curve with equal helix angle cannot meet to the top of ball-end milling cutter, so other shapes of the edge curve must be employed. Chiang and Fong [6] proposed a mathematical method for finding the distribution of cutter body inserts that will result in an equal wear rate for their cutting edges. Jin et al. [7] developed two types of ball-nosed end mill with a unique cutting edge for cutting and finishing hardened steel for practical use. Cheng et al. [8] designed a new microhexagonal end mill, and a polycrystalline diamond microhexagonal end mill with a diameter of 0.5 mm was fabricated by wire electrical discharge machining. Matjaz and Franci and Chen et al. [9, 10] detected and simulated the process of machining ball-end milling. Soo et al. [11] detailed research and development of a Lagrangian-based, 3D finite-element model to simulate the high-speed ball nose end milling of Inconel 718 nickel-based superalloy. Mounayri et al. [12] introduced a special type of artificial neural networks to establish the relationship between the machining conditions (inputs) and process parameters (outputs) for the case of ball-end milling. Tsai and Liao [13] presented a general geometrical model of inclined feed in ball-end

F. Chen (✉) · S. Hu · S. Yin
National Engineering Research Center for High Efficiency Grinding, Hunan University,
Changsha, Hunan 410082, People's Republic of China
e-mail: abccfj@126.com

milling and discussed the influences of different feed angle and helix angle on cutting forces. Lai [14] presented a high-precision manufacturing model for grinding the surface profiles of general ball-end milling cutters. Lai and Chen and Du et al. [15, 16] developed machining methods of cutter. Hsieh [17] presented a set of mathematical models for the design and manufacture of the helical flute and cutting edge curve of a pair of truncated-cone ball-end cutters. Chen and Bin [18] used a cubic boron nitride spherical grinding wheel to grind the rake face of a taper ball-end mill, and the configuration of corresponding computer numerical control (CNC) tool grinder was presented.

Most previous studies only focused on designing the edge curve or the rake face or the rear face, without considering how to realize easy operate and to improve its machining performance. In fact, most cutting edge curves were designed based on operation experience and grinding ability of grinding machine, lack of systematic analysis, modeling, and simulation. Considering the convenience grinding, the rake angle is designed to be various which will make the cutting forces loaded on the cutting edge nonuniform and reduce machining performance. These similar problems will occur while designing and grinding the rear face of ball-end milling cutter.

In this paper, both the rake face with equal normal rake angle and the rear face with equal clearance angle of ball-end milling cutter are designed and modeled, respectively. The new milling cutter may make the flow direction of chip smooth, easily dissipate heat, reduce cutting force, and prevent the chip from scratching machined surfaces. In order to easily grind the rake face and the rear face on a same grinding machine, a new grinding process and mathematical models of the ball-end milling cutter are proposed. A design and simulation software is also developed to optimize various shapes of ball-end milling cutter. A grinding test is carried out to confirm the validation of the mathematical models.

2 Grinding model of the rake face of ball-end milling cutter

2.1 Grinding method of the rake face

In order to easily dress grinding wheel and avoid interference, a conical surface wheel is used on a five-axis linkage grinder as shown in Fig. 1. The grinding movement is shown in Fig. 2 during grinding rake face. The large endface of grinding wheel is always tangent with the edge curve. Ball-end milling cutter rotates clockwise

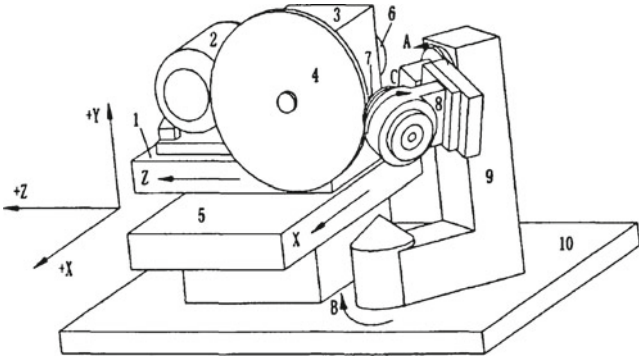

Fig. 1 Structure and coordinate system of five-axis machine. *1* *Z*-axis table, *2* wheel spindle motor, *3* spindle trunk, *4* grinding wheel, *5* *X*-axis table, *6* belt drive unit, *7* ball-end milling cutter, *8* workpiece brace, *9* rotation brace, *10* machine body

with an angular velocity ω_1 around *Y*-axis and rotates counterclockwise with an angular velocity ω_2 around *Z*-axis. Cutter also rotates counterclockwise with an angular velocity ω_3 around *X*-axis. Because the width of rake face from top to bottom is synchronous to be change, grinding wheel has to move along the *X*- and *Z*-axis directions. In the way, the relative motions between grinding wheel and workpiece generate the envelope surface, namely rake face.

2.2 Cutting edge curve model of ball-end milling cutter

Cutting edge curve, an intersecting curve of the rake face and the rear face, is an essential and important factor to design and grind ball-end milling cutter [4, 5], and it is also an orthogonal spiral curve on the sphere. The helix angle of cutting edge curve may improve the sharpness of cutting

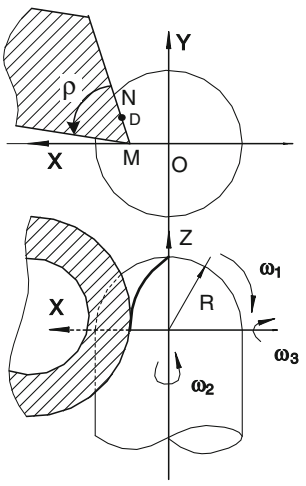

Fig. 2 Forming movement for grinding the rake face

edge. In Fig. 3, the equation of cutting edge curve can be expressed as follows [4, 5]:

$$\mathbf{r} = \left\{ R\cos\varphi\sqrt{1-(c\varphi)^2},\quad R\sin\varphi\sqrt{1-(c\varphi)^2},\quad Rc\varphi \right\},$$
$$c = 1/\tan\omega \tag{1}$$

where R is the radius of ball-end milling cutter and φ is the included angle between the NOZ plane and the XOZ plane. ω is the initial helix angle of cutting edge; in general, the value is 30°. The tangential vector of curve at grinding point N can be also calculated as follows [4, 5]:

$$\mathbf{T} = \left\{ \frac{R(\sin\varphi\cdot c^2\cdot\varphi^2 - \cos\varphi\cdot c^2\cdot\varphi - \sin\varphi)}{\sqrt{1-(c\varphi)^2}},\quad \frac{R(\cos\varphi\cdot c^2\cdot\varphi^2 + \sin\varphi\cdot c^2\cdot\varphi - \cos\varphi)}{\sqrt{1-(c\varphi)^2}},\quad cR \right\} \tag{2}$$

2.3 Rake face model

According to cutting characteristics of edge curve of ball-end milling cutter, the rake face with equal normal rake angle can be regarded as a ruled surface. As shown in Fig. 3, three coordination systems are established. s_0=[O: X, Y, Z] is a structure coordination system of ball-end milling cutter, and O is the center of ball. s_1=[O: X_1, Y_1, Z_1] is a coordination system that s_0 rotates an angle η clockwise around Z-axis. s_2=[O: X_2, Y_2, Z_2] is another coordination system that s_1 rotates an angle θ' clockwise around Y_1-axis.

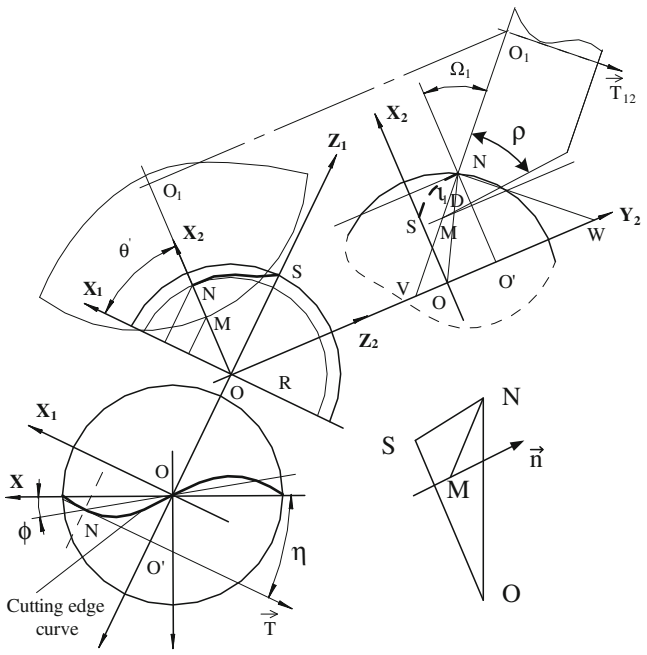

Fig. 3 Mathematical model for grinding the rake face

The transform relationships of these coordination systems are as follows:

$$\begin{bmatrix} X \\ Y \\ Z \end{bmatrix} = \begin{bmatrix} \cos\eta & \sin\eta & 0 \\ -\sin\eta & \cos\eta & 0 \\ 0 & 0 & 1 \end{bmatrix} \begin{bmatrix} \cos\theta' & 0 & -\sin\theta' \\ 0 & 1 & 0 \\ \sin\theta' & 0 & \cos\theta' \end{bmatrix} \begin{bmatrix} X_2 \\ Y_2 \\ Z_2 \end{bmatrix} \tag{3}$$

In Fig. 3, ρ is a conical angle of grinding wheel, S is the top point of ball head, D is a certain point on ruled line MN of the rake face, N is an exterior grinding point on the ball surface, M is an internal grinding point in the ball head, $\boldsymbol{n}$ is the normal vector of the SON plane, Ω_1 is a deflection angle between grinding wheel and cutter, and O_1 is the center of grinding wheel bottom. In specially, the length ON is a rotary radius R_Z in s_0, and the length $O'N$ is expressed as below in s_1:

$$O'N = \sqrt{R^2 - OO'^2} = \sqrt{R^2 - R_Z^2\cdot\sin^2(\eta+\varphi)} \tag{4}$$

In s_2, the coordinates of the point D can be described as follows:

$$\begin{cases} X_2 = R\cdot\sqrt{\cos^2(\eta+\varphi) + c^2\cdot\varphi^2\cdot\sin^2(\eta+\varphi)} - l\cdot\cos\Omega_1 \\ Y_2 = R\cdot\sqrt{1-c^2\cdot\varphi^2}\cdot\sin(\eta+\varphi) - l\cdot\sin\Omega_1 \\ Z_2 = 0 \end{cases} \tag{5}$$

where l is the distance from the point D to the point N. When rotation angle is φ, cutting depth is obtained as follows:

$$\delta_\varphi = \delta + \delta_0 - \delta_0(\delta/\delta_0)^{c\varphi} \tag{6}$$

where δ_0 is an initial cutting depth in the top of ball and δ is a final cutting depth in the root. So, the value range is $0 \le l \le \delta_\varphi$.

2.3.1 The included angle η

According to the grinding method of the rake face, η is an included angle between the tangential vector $\boldsymbol{T}$ and the *XOZ* plane and expressed as follows:

$$\cos < \mathbf{T}, \mathbf{y} >= \frac{\mathbf{T} \cdot \mathbf{y}}{|\mathbf{T}||\mathbf{y}|} = \cos\left(\frac{\pi}{2} - \eta\right) \tag{7}$$

where $\boldsymbol{y}$ is the unit vector along *Y*-axis (that is set in the positive *Y*-direction in this paper), also expressed as follows:

$$\mathbf{y} = \{0,\ 1,\ 0\} \tag{8}$$

Substituting Eqs. 2 and 8 into Eq. 7, we can obtain as follows:

$$\eta = \arcsin\left(\frac{-(\cos\varphi \cdot c^2 \cdot \varphi^2 + \sin\varphi \cdot c^2 \cdot \varphi - \cos\varphi)}{\sqrt{c^4 \cdot \varphi^4 - 2 \cdot c^2 \cdot \varphi^2 + c^2 + 1}}\right) \tag{9}$$

2.3.2 The normal rake angle

From Fig. 3, we can also get as follows:

$$\sqrt{R^2 - R_Z^2 \sin^2(\eta + \varphi)} \cdot \cos\theta' = R_Z \cos(\eta + \varphi) \tag{10}$$

Arranging Eq. 10 gets as follows:

$$\theta' = \arccos\left(\frac{\sqrt{1 - (c\varphi)^2}\cos(\eta + \varphi)}{\sqrt{\cos^2(\eta + \varphi) + c^2 \cdot \varphi^2 \cdot \sin^2(\eta + \varphi)}}\right) \tag{11}$$

According to the definition of the normal rake angle and take into account the geometrical relationship in s_2, the normal rake angle γ_n is the included angle between the ruled line *MN* and the *NOS* plane. In Fig. 3, the coordinate values of the points *N*, *S*, *O*, and *M* are, respectively:

$$\begin{aligned}
&N: \left\{\sqrt{R^2 - R_Z^2 \cdot \sin^2(\eta + \varphi)},\quad R_Z \cdot \sin(\eta + \varphi),\quad 0\right\},\\
&S: \left\{R \cdot \sin\theta',\quad 0,\quad R \cdot \cos\theta'\right\},\\
&O: \{0,\quad 0,\quad 0\},\\
&M: \left\{\sqrt{R^2 - R_Z^2 \cdot \sin^2(\eta + \varphi)} - l \cdot \cos\Omega_1,\quad R_Z \cdot \sin(\eta + \varphi) \cdot l \cdot \sin\Omega_1,\quad 0\right\}.
\end{aligned} \tag{12}$$

So, the equation of the basic surface *NOS* can be obtained as follows:

$$R \cdot \cos\theta' \cdot X + H \cdot Y - R \cdot \sin\theta' \cdot Z = 0 \tag{13}$$

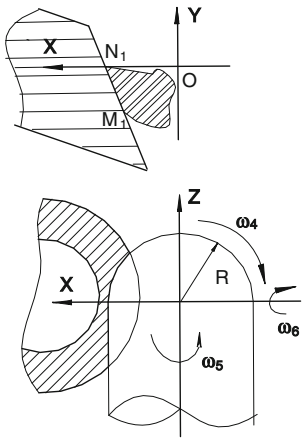

Fig. 4 Forming movement for grinding the rear face

where $H = \frac{-R\sqrt{\cos^2(\eta+\varphi)+(c\varphi)^2\sin^2(\eta+\varphi)}\cdot\cos\theta'}{\sqrt{1-c^2\cdot\varphi^2}\cdot\sin(\eta+\varphi)}$, Form Eq. 13, the normal vector $\boldsymbol{s}$ of the basic surface *NOS* can be calculated:

$$\mathbf{s} = \left\{R \cdot \cos\theta',\quad H,\quad -R \cdot \sin\theta\right\} \tag{14}$$

According to the definition of the normal rake angle, the equation is obtained:

$$\cos\left(\frac{\pi}{2} - \gamma_n\right) = \sin\gamma_n = \frac{|\mathbf{s} \cdot \mathbf{NM}|}{|\mathbf{s}||\mathbf{NM}|} = \frac{-R \cdot \cos\theta' \cdot \cos\Omega_1 - H \cdot \sin\Omega_1}{\sqrt{R^2 + H^2}} \tag{15}$$

So, γ_n can be obtained as follows:

$$\gamma_n = \arcsin\left(\frac{-R \cdot \cos\theta' \cdot \cos\Omega_1 - H \cdot \sin\Omega_1}{\sqrt{R^2 + H^2}}\right) \tag{16}$$

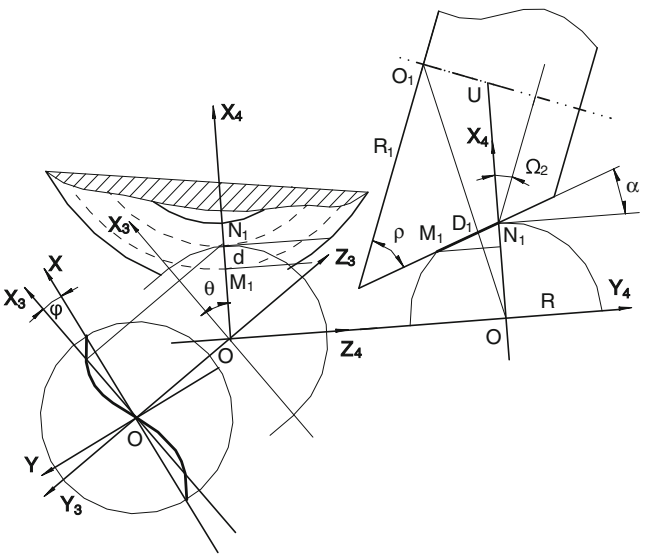

Fig. 5 Mathematical model for grinding the rear face

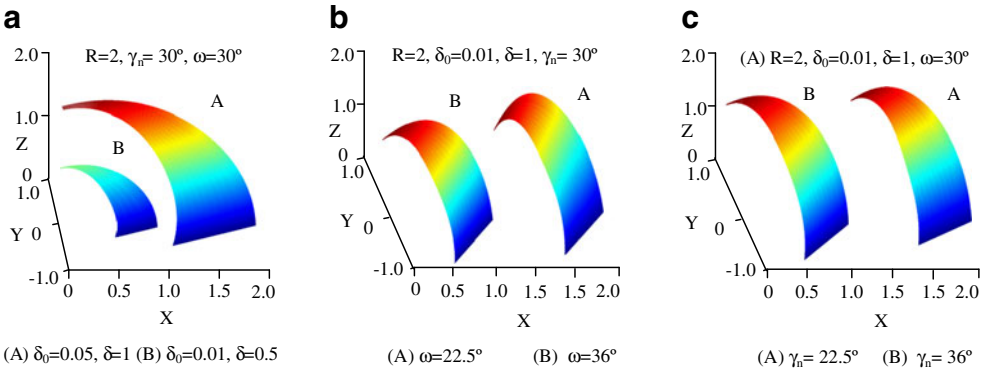

Fig. 6 Simulation and analysis of the rake face (unit millimeters): **a** radius and cutting depth changing; **b** initial helix angle changing; **c** normal rake angle changing

As shown in Eq. 16, the normal rake angle can keep constant by changing other parameters. Substituting Eq. 5 into Eq. 3, we can get the equation of the rake face as follows:

$$\begin{cases} X = \cos\eta\cdot\cos\theta'\cdot\left(R\cdot\sqrt{\cos^2(\eta+\varphi)+(c\cdot\varphi)^2\cdot\sin^2(\eta+\varphi)}-l\cdot\cos\Omega_1\right) \\ \quad +\sin\eta\cdot\left(R\cdot\sin(\eta+\varphi)\cdot\sqrt{1-(c\cdot\varphi)^2}-l\cdot\sin\Omega_1\right) \\ Y = -\sin\eta\cdot\cos\theta'\cdot\left(R\cdot\sqrt{\cos^2(\eta+\varphi)+(c\cdot\varphi)^2\cdot\sin^2(\eta+\varphi)}-l\cdot\cos\Omega_1\right) \\ \quad +\cos\eta\cdot\left(R\cdot\sin(\eta+\varphi)\cdot\sqrt{1-(c\cdot\varphi)^2}-l\cdot\sin\Omega_1\right) \\ Z = \sin\theta'\cdot\left(R\cdot\sqrt{\cos^2(\eta+\varphi)+(c\cdot\varphi)^2\cdot\sin^2(\eta+\varphi)}-l\cdot\cos\Omega_1\right) \end{cases} \tag{17}$$

According to the symmetry of ball-end milling cutter, the surface equation of another rake face can be also obtained, and it is not described in detail here.

3 Grinding model of the rear face of ball-end milling cutter

3.1 Grinding method of rear face

The same conical grinding wheel is used to grind the rear face on the same grinder, and the grinding movement is also shown in Fig. 4. The external conical surface of grinding wheel is always tangent with the edge curve. Ball-end milling cutter rotates clockwise with an angular velocity ω_4 around Y-axis and rotates counterclockwise with an angular velocity ω_5 around Z-axis. The cutter also rotates counterclockwise with an angular velocity ω_6 around X-axis. Meanwhile, grinding wheel should move along the X- and Z-axis directions. In this way, the relative motion between grinding wheel and workpiece can generate a rear face.

3.2 Rear face model

The modeling method of rear face with equal clearance angle is similar with rake face. As shown in Fig. 5, three coordination systems are established. s_0=[O: X, Y, Z] is the structure coordination system of ball-end milling cutter. s_3=[O: X_3, Y_3, Z_3] is a coordination system that s_0 rotates an angle φ counterclockwise around Z-axis. s_4=[O: X_4, Y_4, Z_4] is another coordination system that s_3 rotates an angle θ clockwise around Y_3-axis. The transform relationships of these coordination systems are as follows:

$$\begin{bmatrix} X \\ Y \\ Z \end{bmatrix} = \begin{bmatrix} \cos\varphi & -\sin\varphi & 0 \\ \sin\varphi & \cos\varphi & 0 \\ 0 & 0 & 1 \end{bmatrix} \begin{bmatrix} \cos\theta & 0 & -\sin\theta \\ 0 & 1 & 0 \\ \sin\theta & 0 & \cos\theta \end{bmatrix} \begin{bmatrix} X_4 \\ Y_4 \\ Z_4 \end{bmatrix} \tag{18}$$

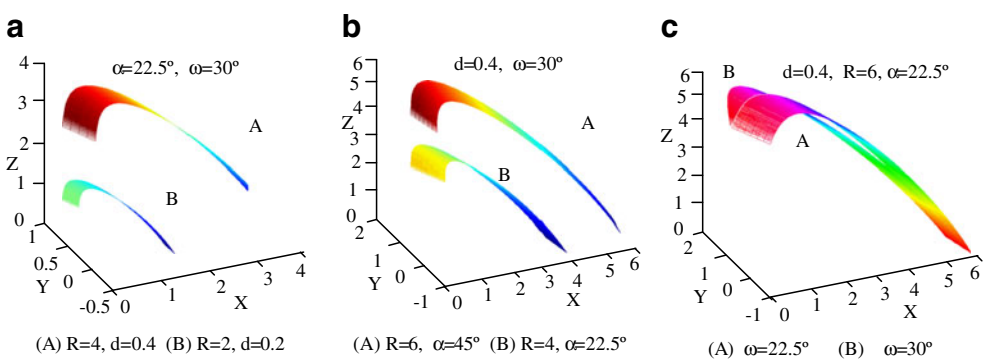

Fig. 7 Simulation and analysis of the rear face (unit millimeters): **a** radius and width changing; **b** radius and clearance angle changing; **c** initial helical angle changing

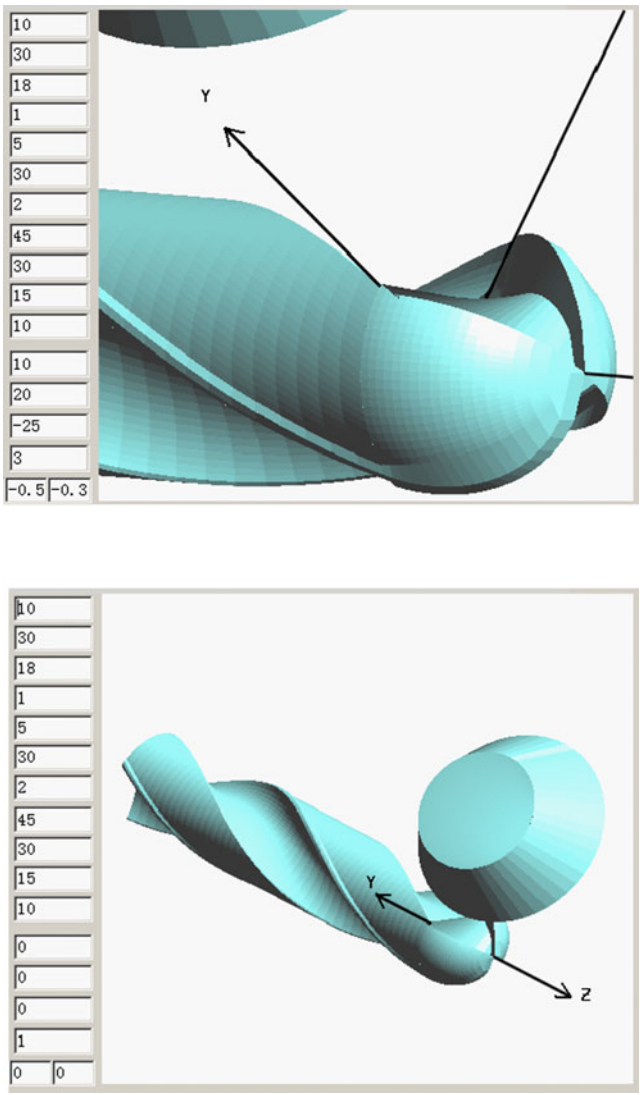

Fig. 8 3D design and simulation of ball-end milling cutter: **a** 3D-design of ball-end milling cutter; **b** grinding simulation of cutter in 3D

In Fig. 5, d is the width of the rear face, α is the clearance angle, and D_1 is a certain point on grinding line MN. Ω_2 is the deflection angle between the grinding wheel and the cutter and can be expressed as follows:

$$\Omega_2 = \pi/2 - \rho - \alpha \tag{19}$$

As shown in Eq. 19, the clearance angle can keep constant by changing other parameters. According to Eq. 2, the parameter θ can be expressed by θ=arcsin($c\varphi$). The coordinates of the point D_1 can be obtained in the s_4, as follows:

$$\{X_4,\ Y_4,\ Z_4\} = \{R - l_\alpha \cdot \sin\alpha,\ l_\alpha \cdot \sin\alpha,\ 0\}, 0 \le l_\alpha \le d \tag{20}$$

where l_α is the distance from the grinding point D_1 to the point N_1. Substituting Eq. 20 into Eq. 18, the surface equation of the rear face can be obtained as follows:

$$\begin{cases} X = (R - l_\alpha \cdot \sin\alpha) \cdot \cos\varphi \cdot \sqrt{1 - (c \cdot \varphi)^2} + l_\alpha \cdot \cos\alpha \cdot \sin\varphi \\ Y = (R - l_\alpha \cdot \sin\alpha) \cdot \sin\varphi \cdot \sqrt{1 - (c \cdot \varphi)^2} - l_\alpha \cdot \cos\alpha \cdot \cos\varphi \\ Z = (R - l_\alpha \cdot \sin\alpha) \cdot c \cdot \varphi \end{cases} \tag{21}$$

According to the symmetry of ball-end milling cutter, the surface equation of another rear face can be also obtained.

Fig. 9 External view of five-axis grinder

4 Simulation analysis of the rake face and rear face

According to the above mathematical models, the shape of the rake face is decided by some parameters such as the ball radius R, the initial helix angle ω, the normal rake angle γ_n, the initial cutting depth δ_0 in the top of ball, and the final cutting depth δ in the root. A simulation analysis on the rake face is carried out by changing the parameter φ from zero to the maximum value tan(ω). Figure 6 shows the different shapes of the rake face of ball-end milling cutter by changing δ_0, δ, ω, and γ_n, respectively. From Fig. 6, the helix angle

Fig. 10 The rake face and rear face **a** before and **b** after ground

ω and the normal rake angle γ_n have the most significant influence on the rake face.

Similarly, from the mathematical model of the rear face, it is known that the shape of the rear face is decided by some parameters such as the ball radius R, the initial helix angle ω, and the clearance angle α. The simulation analysis on the rear face is carried out by changing the basic parameter φ. Figure 7 shows the different shapes of the rear face of ball-end milling cutter by changing R, α, and ω, respectively. From Fig. 7, the helix angle ω and the clearance angle α have the most significant influence on the rear face.

In order to verify the grinding model and obtain an optimal visual design about the ball-end milling cutter, a 3D interactive simulation and design software is developed. As shown in Fig. 8a, ball-end milling cutter with various shapes can be obtained by changing corresponding parameters in this design simulation software. Ball-end milling cutter can be visualized and reviewed by translation, rotation, scaling, and other transform controls in the 3D software. In Fig. 8b, the animation simulation process that a conical grinding wheel grinds the rake face with equal normal rake angle of ball-end milling cutter can be also shown.

5 Grinding experiment of ball-end milling cutter

Based on the above mathematical models and simulation results of ball-end milling cutter with equal rake angle and rear angle, a grinding experiment is carried out on five-axis tool grinder. Figure 9 shows the external view of this machine which includes two linear axes (X, Z) and three rotation axes (A, B, C). The travel angle of A-axis is from 0° to 90°, B-axis is from 0° to 180°, C-axis is from 0° to 360°, and the resolution of A–B–C-axis is 0.001°. The linear stroke of Z-axis is 150 mm, and the one of X-axis is 120 mm. The conical hard grinding wheel with diameter 400 mm is used, and the maximum rotation speed is 2,000 rpm. The ground workpiece is a cutter with equal rake angle and rear angle. The diameter is 10 mm, and the material is cemented carbide. The comparison between before and after ground ball-end milling cutter is shown in Fig. 10. Before ground, the wears of the rake face, cutting edge, and rear face are obvious, after these wear areas are reground by the five-axis grinder; however, the new rake and rear faces are emerged, and the cutting edge is sharp again. The test result shows the ball-end milling cutter with equal rake angle and rear angle can be ground on five-axis grinder based on above mathematical models. However, it is difficult and unnecessary to measure the every different rake face and rear face after ground; in fact, it only needs to meet the approximately requirements. The performance optimizing the ball-end milling cutter can be conducted by lots of milling experiments, which will be carried out in our future research work.

6 Conclusions

According to the grinding characteristics of ball-end milling cutter, new grinding method and mathematical model of ball-end milling cutter are developed, and some conclusions can be obtained:

1. Both the rake face with equal normal rake angle and the rear face with equal clearance angle are designed. These equal angles make cutting forces uniform, improve escape of chips, reduce resistance, and enhance machining performance of ball-end milling cutter.
2. New grinding method is developed to grind the rake face and the rear face of ball-end milling cutter by using a CNC platform with five-axis linkage.
3. A conical surface wheel is employed to grind the ball-end milling cutter. The large endface of grinding wheel can be used to grind the rake face. Of course, the external conical surface of the same wheel is for the rear face.
4. Mathematical models of both the rake face with equal normal rake angle and the rear face with equal clearance angle are established. The validity of the models is also verified by simulation results and experimental test.

References

1. Wu CT, Chen CK, Tang YY (2001) Modelling and computer simulation of grinding of the ball end type rotating cutter with a constant helical angle. Proc Inst Mech Eng Part B: Eng Manuf 215 (11):1581–1594
2. Engin S, Altina Y (2001) Mechanics and dynamics of general milling cutters. Part I: helical end mills. Int J Mach Tools and Manuf 41(15):2195–2212
3. Altinta Y, Engin S (2001) Generalized modelling of mechanics and dynamics of milling cutters. CIRP Ann 50(1):25–30
4. Chen WF (2004) A mathematical solution to the design and manufacturing problems of ball-end milling cutters having a cutting edge with constant angle to the axis. Proc Inst Mech Eng Part C: J Mech Eng Sci 218(3):301–308
5. He YX, Zhou YF, Zhou J (2002) Generalized helical movement and geometric modelling of complicated-shape revolving cutting tools. Acta Aeronaut Astronaut Sin 23(2):135–139
6. Chiang CJ, Fong ZH (2010) Design of form milling cutters with multiple inserts for screw rotors. Mechanism and Machine Theory 45:613–1627
7. Jin M, Goto I, Watanabe T, Kurosawa JI, Murakawa M (2007) Development of cBN ball-nosed end mill with newly designed cutting edge. J Mater Process Technol 192–193:48–54
8. Cheng X, Wang ZG, Nakamoto K, Yamazaki K (2011) A study on the micro tooling for micro/nano milling. Int J Adv Manuf Technol 53:523–533

9. Matjaz M, Franci C (2003) Simulation of cutting forces in ball-end milling. Robot and Comput Integr Manuf 19(2):99–107
10. Chen WY, Chang PC, Liaw SD (2005) A study of design and manufacturing models for circular-arc ball-end milling cutters. J Mater Process Technol 161(3):467–477
11. Soo SL, Dewes RC, Aspinwall DK (2010) 3D FE modelling of high-speed ball nose end milling. Int J Adv Manuf Technol 50:871–882
12. Mounayri HE, Briceno JF, Gadallah M (2010) A new artificial neural network approach to modeling ball-end milling. Int J Adv Manuf Technol 47:527–534
13. Tsai CL, Liao YS (2010) Cutting force prediction in ball-end milling with inclined feed by means of geometrical analysis. Int J Adv Manuf Technol 46:529–541
14. Lai HY (2002) A high-precision surface grinding model for general ball-end milling cutters. Int J Adv Manuf Technol 19(6):393–402
15. Lai HY, Chen WF (2002) Precision design and numerical control machining of tapered ball-end milling cutters. Proc Inst Mech Eng Part B: Eng Manuf 216(2):183–197
16. Du SJ, Surmann T, Webber O (2005) Formulating swept profiles for five-axis tool motions. Int J Mach Tools and Manuf 45(7–8):849–861
17. Hsieh JM (2008) Manufacturing models for design and NC grinding of truncated-cone ball-end cutters. Int J Adv Manuf Technol 35 (11–12):1124–1135
18. Chen F, Bin HZ (2009) A novel CNC grinding method for the rake face of a taper ball-end mill with a CBN spherical grinding wheel. Int J Adv Manuf Technol 41:846–857